Advanced High-Voltage Electrolyte Design Using Poly(ethylene oxide) and High-Concentration Ionic Liquids for All-Solid-State Lithium Metal Batteries

Mingjie Zhang[a,c], Urbi Pal[c*], Faezeh Makhlooghiazad[c], Luke A. O'Dell[c], Shinji Kondou[c], Giuseppe A. Elia[a,b], Claudio Gerbaldi[a,b*], and Maria Forsyth[c]

[a]GAME Lab, Department of Applied Science and Technology (DISAT), Politecnico di Torino, Corso Duca degli Abruzzi 24, 10129, Torino, Italy
[b]National Reference Center for Electrochemical Energy Storage (GISEL) - INSTM, Via G. Giusti 9, 50121, Firenze, Italy
[c]Institute for Frontier Materials (IFM), Deakin University, Burwood, Victoria 3125, Australia.

*u.pal@deakin.edu.au, claudio.gerbaldi@polito.it

Abstract

Poly(ethylene oxide) (PEO) based solid polymer electrolytes (SPEs) are one of the most promising materials for solid-state lithium metal batteries (LMBs) due to their inherent safety advantages, however, they suffer from insufficient room temperature ionic conductivity (up to 10^{-6} S cm^{-1}) and limited oxidation stability (< 4V). In this study, a novel "polymer-in-high concentrated ionic liquid" (PiHCIL) electrolyte composed of PEO, N-propyl-N-methylpyrrolidinium bis(fluorosulfonyl) imide (C$_3$mpyrFSI) ionic liquid (IL) and LiFSI is designed. The EO: [Li/IL] ratio has been widely varied and their physical and electrochemical properties have been explored. The Li-coordination and solvation structure has been explored through FTIR spectroscopy and solid-state magic angle spinning (MAS) NMR. The designed electrolyte provides promisingly high oxidative stability of 5.1V and offers high ambient temperature ionic conductivity of 5.6 x10^{-4} S cm^{-1}. Li|Li symmetric cell cycling showed very stable and reversible cycling of Li metal over 100 cycles and smooth, dendrite-free deposition morphology. All-solid-state cells using composite LFP cathode exhibited promising cycling with 99.2% capacity retention at C/5 rate over 100 cycles. Therefore, the novel approach of PiHCIL enables a new pathway to design high-performing SPEs for high-energy density all-solid-state LMBs.

1. Introduction

Solid-state lithium metal batteries (LMBs) are recognized as the future of energy storage technology, offering unparalleled energy densities and safety that far exceed those of current lithium-ion batteries[1]. However, the widespread adoption of solid-state LMBs in sectors such as electric vehicles, electric aviation and energy storage is hindered by significant challenges, particularly in the development of electrolyte materials. Among different types of solid electrolytes, solid polymer electrolytes (SPEs) stand out as promising candidates due to their inherent safety and processibility advantages as well as the potential to facilitate high energy LMBs.[2,3] Unfortunately, the majority of SPEs require plasticization with a liquid solvent to improve their intrinsically low ionic conductivity and poor wettability, which not only compromises the mechanical properties but also introduces safety concerns similar to those of liquid electrolytes such as leakage and flammability.[4–6] Consequently, designing all-solid-state SPE systems that maintain both high ionic conductivity and mechanical integrity remains a significant challenge.

Poly(ethylene oxide) (PEO) has become the leading material for SPEs since the 1970s because of its exceptional coordination and dissociation ability towards Li salt, excellent interfacial stability with Li metal, and high mechanical strength to form flexible membranes.[7,8,9] Specifically, high molecular weight PEO shows the advantages of preventing Li dendrites and improved cycling stability due to its prominent mechanical property compared to lower molecular weight PEO.[10] However, PEO-based SPEs are often criticized for their limited electrochemical stability window (ESW) primarily owing to the low oxidative stability of ether oxygen and limited room temperature ionic conductivity (up to 10^{-6} S cm^{-1}) due to their crystallization tendency that restricts polymer segmental motion for ion transport.[9] These limitations significantly restrict their operational voltage range (< 4V) and fast cycling capability in solid-state LMBs. Intensive research has been centred on enhancing ionic conductivity and oxidative stability of PEO-based SPEs, such as applying inorganic fillers,[11–13] plasticizing ionic liquids,[14] designing complex polymer architecture and single-ion conducting polymers,[15–18] and introducing crosslinked networks.[19,20] Among these, ionic liquid (IL)-based electrolytes have received significant interest because of their good electrochemical and thermal stability, low vapor pressure, and non-flammability.[21] Early works from Howlett et al. and other researchers demonstrated promising physical and electrochemical properties of ILs as the electrolyte solvent for LMB applications.[22–24] Susan et al. have successfully incorporated ionic liquids with compatible polymers for the preparation of "ion gels", showing increased thermal stability and high ambient temperature conductivity.[25] In recent years, enlightening from the idea of concentrated electrolyte in liquid electrolytes,[26–28] research has identified high salt concentration ionic liquid electrolyte as a novel approach to effectively enhance Li ion transport, electrochemical stability, and support fast charge-discharge.[29,30] Pal et al. and co-workers investigated an ether-aided super concentrated ionic liquid electrolyte that could effectively enhance ion transport and interfacial stability toward Li metal and high voltage materials.[31–33] With the ever-increasing attempt to boost the performance of SPEs, the use of high concentrated salt-IL mixtures is predicated to improve both electrochemical stability and ion transport of PEO-based SPEs by altering the ion dynamics and creating more efficient Li transport pathways within the polymer matrix.

Although properties of binary IL electrolytes (i.e., either salt-IL or polymer-IL) have been extensively studied, the complex properties of 'ternary systems' composed of a polymer and a high concentration salt-IL mixture (HCIL) have been less explored. In this work, we report a novel PEO-in-high salt concentrated ionic liquid system (PiHCIL-SPE) based on LiFSI and

C$_3$mpyrFSI ionic liquid. We studied the effect of HCIL concentration on the physical and electrochemical properties of the composite electrolyte. By focusing on the enhancement of electrochemical window and ion transport, we seek to address a critical gap in the current understanding of PEO-based SPEs. Fourier-transform infrared spectroscopy (FTIR) and solid-state MAS NMR techniques are used to unravel the cation-polymer and cation-anion interactions and their impacts on ion dynamics within the designed SPEs. The optimal PiHCIL-SPE achieved high electrochemical stability and ambient temperature ionic conductivity. Stable and reversible cycling toward Li metal electrodes and favourable all-solid-state LMB performance were demonstrated. Based on the findings, an ion conduction network model consisting of interconnected ion clusters and pores is proposed to help understand the high ionic conductivity, and promising battery performance of the designed PiHCIL-SPE. Thus, we believe the concept of incorporating high salt-concentrated IL into high molecular weight PEO to form a robust SPE represents a promising approach toward safer and high-performing all-solid-state LMBs.

2. Experimental Section

2.1 Materials

Poly(ethylene oxide) (PEO, M$_w$ 5,000,000, Sigma-Aldrich) was dried under vacuum at 50 °C for 24 h before use. N-propyl-N-methylpyrrolidinium bis(fluorosulfonyl) imide (C$_3$mpyrFSI) (purity 99.5%) from Solvionic and lithium bis(fluorosulfonyl)imide (LiFSI) from Nippon Shokubai were dried under vacuum at 50 °C for 48 h before use. Lithium iron phosphate (LFP) powder was purchased from Custom Cells, lithium manganese oxide (LMO) was supplied from Calix Ltd and Super C65 carbon was purchased from Sigma. All materials were kept in an argon-filled glove box for further SPE preparation.

2.2 Solid Polymer Electrolyte Membrane Preparation

The PiHCIL-SPEs were prepared using solvent casting within an argon-filled glovebox as shown in **Figure 1**. First, LiFSI and C$_3$mpyrFSI (LiFSI:IL molar ratio equal to 1:1) were mixed and fully dissolved. The obtained solution was then mixed with various amounts of PEO in acetonitrile to form SPEs with EO:Li:IL molar ratios equal to 8:1:1, 10:1:1, 15:1:1 and 20:1:1. The obtained mixtures were then cast into silicon moulds inside the glovebox (MBraun UNILab, H$_2$O and O$_2$ content <1 ppm) and rested for 48 h to ensure slow solvent evaporation. The obtained solid membranes were then put between two Mylar sheets and hot pressed (70°C, 2 MPa, 10 mins) to obtain a homogenous, free-standing and pin-hole free SPE with a thickness of 120 ± 10 μm. The membranes were transferred to a Buchi oven and vacuum-dried at 50 °C for another 24 h before further characterization and cell assembly. The SPEs are named as PiHCIL-SPE$_{x:1:1}$ where x is the polymer content.
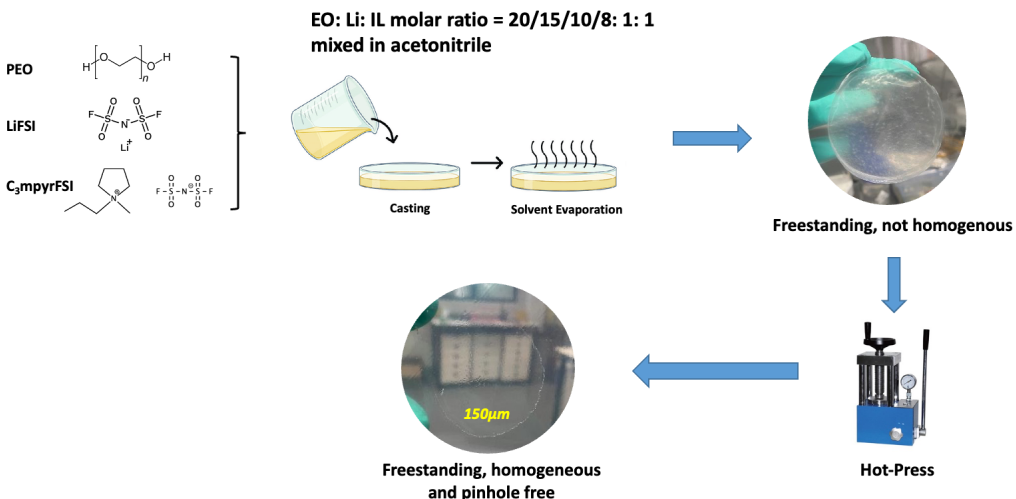
Figure 1. Free-standing PiHCIL-SPE membrane preparation by solvent casting.

2.3 Characterization techniques

Differential Scanning Calorimetry (DSC) (Mettler Toledo DSC1) was used to investigate the phase behaviour of the prepared PiHCIL-SPEs in the temperature range of -120 to 80 °C. A 10 °C min^{-1} heating and 20 °C min^{-1} cooling rate was used and the sample loading was about 15 mg.

Electrochemical impedance spectroscopy (EIS) analysis (MTZ-35 impedance analyser, Biologic) was used to measure ionic conductivity (σ) of the PiHCIL-SPEs. The measurements were conducted over a temperature range of 20-70 °C in frequency from 0.1Hz to 1 MHz. A SS|PiHCIL-SPEs|SS (stainless-steel) coin cell configuration was used. The bulk resistance was calculated from the impedance curve at high frequency, and the ionic conductivity was calculated based on the following equation:

$$\sigma = \frac{l}{R_b \cdot A}$$

where σ is the ionic conductivity (S cm^{-1}), R_b is the bulk resistance (derived from the impedance curve), l is the membrane thickness and A is the area.

Fourier transform infrared (FTIR) spectra were obtained at room temperature in argon atmosphere using a Perkin Elmer Spectrum 400. Thirty-two scans from to 650 to 4000 cm^{-1} were accumulated per sample.

Thermal gravimetric analysis (TGA) was performed using a Mettler Toledo TGA STAR instrument to understand the thermal decomposition of the membranes with a sample loading of 10 mg. Mass loss was recorded over 30-600 °C with a 10 °C min^{-1} heating rate under constant N$_2$ flow.

Scanning electron microscope (SEM) analysis was carried out for the pristine PiHCIL-SPEs as well as cycled cells. A coin cell disassembly unit (Hohsen) was used inside glove-box to disassemble the cycled cells. The JSM-IT300 SEM from JEOL (Japan) was used to study the surface and cross-section morphology with a 10 kV acceleration voltage.

Solid-State Magic Angle Spinning (MAS) NMR Spectroscopy technique was used to probe the cation-polymer and cation-anion interactions. Zirconia MAS rotors (2.5 mm diameter) were used to pack the samples inside an argon glovebox. A Bruker 2.5 mm HXY probe

spinning at 25 kHz under a 11.7 T magnetic field (500 MHz ^{1}H frequency) was used to carry out the experiment. One-dimensional ^{7}Li and ^{19}F spectra were obtained by a single-pulse experiment. Additionally, a two-dimensional ^{19}F$-^7$Li heteronuclear correlation (HETCOR) spectrum was acquired.

2.4 Electrode Preparation, Cell Assembly and Electrochemical measurements

The composite LFP (c-LFP) and LMO (c-LMO) electrodes were prepared by mixing LFP or LMO powder, Super C65 and our prepared SPE$_{20:1:1}$ as the binder in 80:10:10 wt% in acetonitrile. The slurry was mixed until smooth and cast using a doctor-blade on carbon-coated aluminium foil. The obtained c-LFP and c-LMO electrodes have an average cathode mass loading of 2.5 and 3 mg cm^{-2} and an areal capacity of 0.46 and 0.45 mAh cm^{-2}, respectively. The composite cathodes were then cut into 8 mm diameter discs and vacuum-dried at 50 °C for 24 h prior to cell assembly.

For all the battery measurements, lithium metal (100 μm, Gelon) was used as anode material and current collector. The all-solid-state batteries were then assembled using a Li metal anode, a free-standing SPE$_{8:1:1}$ membrane, and the prepared composite cathodes (c-LFP and c-LMO).

A multi-channel potentiostat VMP3 (BioLogic) was used to conduct the electrochemical measurements. Li transference number (tLi+) is measured using a Li|Li symmetric cell at 70 °C and calculated using the Bruce-Vincent equation:

$$t_{Li+} = \frac{I_s \ (\Delta V - I_0 R_0)}{I_0 \ (\Delta V - I_s R_s)}$$

where ΔV is the applied voltage (10 mV polarization), R$_0$ and R$_s$ are the charge transfer resistances of the initial and steady-state phases, respectively, and I$_0$ and I$_s$ are currents in initial and steady-state stage, respectively.

The galvanostatic cycling for Li||Li, Li||LFP/c-LFP, and Li||LMO/c-LMO cells were also carried out. All electrochemical measurements were conducted using CR2032 coin cells (Hohsen Corp.). Cell cycling was carried out at 50 °C with voltage limits of 2.5 to 4 V for Li/c-LFP cells, and 3 to 4.3 V for Li/c-LMO cells. Two formation cycles at C/20 were used before long-term cycling unless mentioned otherwise. The reproducibility of the results has been checked by multiple tests.

3. Results and Discussion

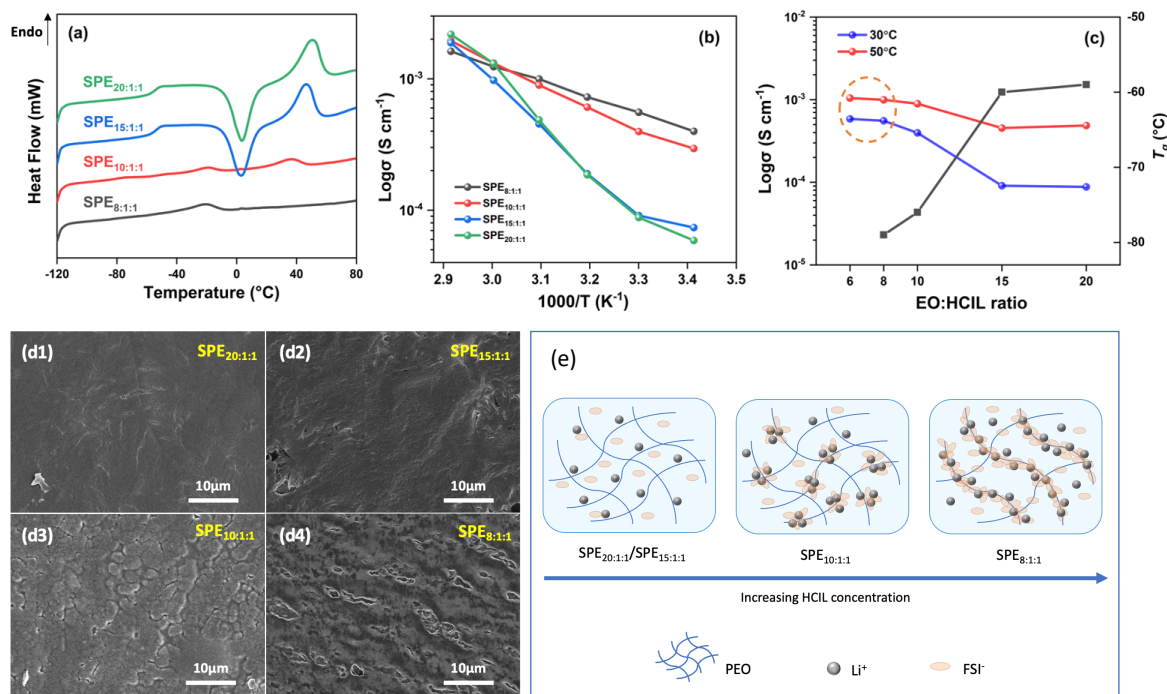## 3.1. Phase Behaviour, Ionic Conductivity and Microstructure

Figure 2. (a) Phase behavior of different PiHCIL-SPE systems obtained from DSC measurements. (b) Ionic conductivities of different PiHCIL-SPE systems in the temperature range 20–70°C. (c) Ionic conductivities of the PiHCIL-SPEs at 30 and 50 °C and their T_g as a function of EO:HCIL ratio. (d) SEM revealing the surface morphology of different PiHCIL-SPEs. (e) Schematic morphology models of different PiHCIL-SPEs systems.

Figure 2 provides an overview of PiHCIL-SPEs where the relative ratio of PEO and high salt content ionic liquids (HCIL) influences the phase behavior, ionic conductivity, and morphology. It is established that PEO is a semi-crystalline polymer with a melting transition at 65 °C.[7] As shown in Figure 2a, the addition of HCIL to PEO in a 20:1:1 molar ratio reduces the melting transition temperature to 50 °C and introduces a T_g at -55°C, indicating the coexistence of amorphous and crystalline phases in $SPE_{20:1:1}$. Increasing the HCIL ratio to 10:1:1 further lowers the melting transition in both temperature and enthalpy, accompanied by a significant reduction in T_g (-76 °C). This notable decrease in T_g in $SPE_{10:1:1}$, compared to $SPE_{20:1:1}$ or $SPE_{15:1:1}$, likely results from altered interactions between the polymer chains and the Li^+ ions in the presence of FSI^- anions which will be further discussed. At an even higher HCIL ratio of 8:1:1, the melting peak disappears, and the T_g drops further to -79 °C, suggesting a highly amorphous phase. Notably, in samples with higher HCIL ratios ($SPE_{8:1:1}$, and $SPE_{10:1:1}$), a small peak at approximately -20°C appears, attributed to a phase transition in the $C_3mpyrFSI/LiFSI$ ionic liquid, which indicates the solubility limit of the IL in PEO and potential phase separation.[30,34]

The impact of HCIL on the ionic conductivity of the prepared SPEs is detailed in **Figure 2b and c**. There is a clear dependency of conductivity on HCIL concentration. The conductivity values for $SPE_{20:1:1}$ and $SPE_{15:1:1}$ are remarkably similar, aligning with their comparable melting transitions and T_g values (Fig. 1a). They exhibit a sharp increase in ionic conductivity from the order of 10^{-5} S cm^{-1} at 30 °C to 10^{-3} S cm^{-1} at 70 °C, consistent with the DSC data showing a melting transition at 35 °C (onset) to 65 °C (end). Furthermore, there is a significant rise in ionic conductivity from $SPE_{15:1:1}$ (9.1 x10^{-5} S cm^{-1} at 30 °C) to

SPE$_{10:1:1}$ (4 x10^{-4} S cm^{-1} at 30 °C) and SPE$_{8:1:1}$ (5.56 x10^{-4} S cm^{-1} at 30 °C), suggesting that HCIL enhances overall ionic mobility. This is confirmed by DSC data, where the crystallization peak diminishes for SPE$_{10:1:1}$ and disappears for SPE$_{8:1:1}$. No gain in ionic conductivity is observed above 8:1:1 ratio (Fig. 2c and Fig. S1) and excess IL starts to exude from the polymer matrix in SPE$_{6:1:1}$ (Fig. S2), indicating a potential HCIL solubility limit in the PEO chain.[35] Therefore, we speculate that SPE$_{8:1:1}$ represents an optimal EO:Li:IL ratio, favoring high ambient temperature ionic conductivity which is closely approximating that of HCIL liquid electrolytes.[31]

The surface morphology of the prepared PiHCIL-SPEs was characterized by SEM and shown in **Figure 2d**. With high PEO content and low HCIL presence (i.e., SPE$_{20:1:1}$ and SPE$_{15:1:1}$), the SPEs show a relatively dense and smooth surface (Fig. d1 and d2), highlighting the good miscibility of PEO and HCIL. With decreasing PEO content, a heterogeneous microstructure is observed (Fig. d3), indicating the formation of separated phases, most likely approaching the miscibility limit of HCIL into the polymer. When the ratio reaches 8:1:1, a porous, interconnected and aligned ion conducting network is formed (Fig. d4). It can be proposed that at high polymer content, most LiFSI can be dissociated by the PEO backbone, and most FSI$^-$ anions exist as free ions. Li$^+$ ions mainly transfer via chain segmental motion.[36] Therefore, ionic conductivity increases slowly with increasing HCIL content due to increased charge carrier amounts; whereas at low polymer content, and high HCIL content, a considerable amount of LiFSI cannot be dissociated, and together with the anions from the IL they can form aggregated ion clusters, resulting in phase separation and pores in the system. The ion conduction behavior in this case can be explained by a "polymer-in-salt" percolation model where high salt content favors the formation of an ion conductive network composed of interconnected ion clusters that provide percolation pathways for fast ion transport.[37,38] Consistent with the polymer-in-salt system,[36] in SPE$_{8:1:1}$, the excessive FSI$^-$ anions from both LiFSI and C$_3$mpyrFSI form interconnected cluster networks and pores as shown in Fig. d4. Interestingly, these connected ion clusters and pores also happen to be locally aligned, which can provide direct pathways for Li$^+$ transport, reducing tortuosity. This can lead to more efficient ion transport and higher conductivity. The pores may help accommodate volume change during cell cycling, potentially enhancing mechanical stability and longevity of the SPE. **Figure 2e** shows a proposed morphology model to help understand the structural change and ion dynamics in the prepared PiHCIL-SPEs.

3.2. Coordination environment through FTIR and MAS solid-state NMR
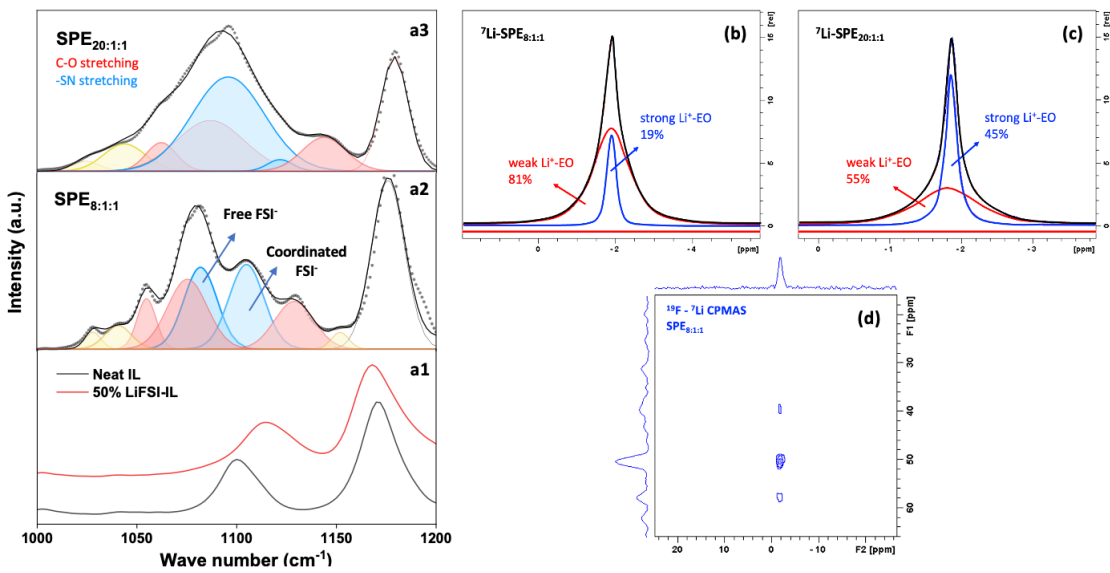

Figure 3. (a) FTIR spectra of SPE$_{8:1:1}$ and SPE$_{20:1:1}$. Neat IL and 50 mol% LiFSI-IL were measured for reference. (b,c) Deconvoluted ^{7}Li solid-state MAS NMR spectra of SPE$_{8:1:1}$ and SPE$_{20:1:1}$. (d) ^{19}F–^{7}Li HETCOR spectrum of SPE$_{8:1:1}$.

FTIR was used to investigate the changes of cation-polymer and cation-anion interactions in the prepared PiHCIL-SPEs as shown in **Figure 3a** (the full spectrum is given in **Fig. S3**, supporting information). In the region between 1000 and 1200 cm^{-1}, a vibrational peak at 1100 cm^{-1} from the neat IL (Fig. a3) is assigned to the -SNS symmetric stretching from the FSI$^-$ anions.[39] Our previous work showed that adding 50 mol% LiFSI salt to the neat IL shifted this peak to 1115 cm^{-1} which was attributed to the increased coordination between Li$^+$ and FSI$^-$ anions.[31] After adding PEO (Fig. a2), the -SNS stretching peak shifts to lower wavenumbers and splits into free FSI$^-$ and coordinated FSI$^-$ (blue), indicating a coordination environment change of the FSI$^-$ anions that may be due to the introduced Li$^+$-EO coordination in SPE$_{8:1:1}$. As PEO content increases, the coordinated FSI$^-$ peak dramatically decreased leaving mainly free FSI$^-$ in the SPE$_{20:1:1}$ (Fig. a3). Additionally, three -CO stretching peaks (red) from PEO shifted to higher wavenumbers, suggesting a coordination environment change of the -CO groups which may be due to increased Li$^+$-EO coordination and this is consistent with PEO-salt systems.[40,41] Therefore, summarily it can be stated that increasing HCIL concentration in the PEO matrix results in more coordinated FSI$^-$ anions, leading to the formation of a connected anion-rich ion conducting phase that can be further supported by the microstructure analysis in **Figure 2d**. These separated phases might also decrease the crystalline regions of PEO, leading to higher chain mobility, improving the ionic conductivity and thus faster Li$^+$ transport.

To further illustrate the Li$^+$ coordination environment in the PiHCIL-SPEs, solid-state MAS NMR experiments were performed. Analysis of the asymmetric ^{7}Li signals (**Figure S4a**) shows two Li$^+$ environments (**Figure 3b and c**). Consistent with Greenbaum's work,[42] the right peak (45% of total integral) in SPE$_{20:1:1}$ is assigned to the Li$^+$ ions closely bound to the EO units which can be considered as solvated Li$^+$. The left peak (55% of total integral) represents Li$^+$ ions that have weakened Li$^+$-EO interactions which are less restricted and behave more as in ionic states. As HCIL concentration increases, SPE$_{8:1:1}$ shows 81% weakly coordinated Li$^+$ and only 19% strongly bonded Li$^+$, indicating more Li$^+$ ions escape from strong Li$^+$-EO interactions to the disordered environment where they possess a higher

degree of freedom. Thus, the addition of HCIL can mitigate the affinity between EO and Li^+ interaction which is consistent with the FTIR results. Previous research has shown that Li^+ ions are more mobile in disordered environments, promoting faster ion transport.[43] This is consistent with our EIS analysis where $SPE_{8:1:1}$ shows the highest ionic conductivity. The close interactions between Li^+ and FSI^- anions are established in the $^{19}F-^7Li$ HETCOR spectrum shown in **Figure 3d**, where ^{19}F shows strong cross peaks with the ^7Li signal. Taken together, solid-state NMR results confirm the important role of Li^+ environment to the overall ionic conductivity. The favorable Li^+ ion environment of $SPE_{8:1:1}$ promotes its superior room temperature ionic conductivity among the prepared PiHCIL-SPEs.
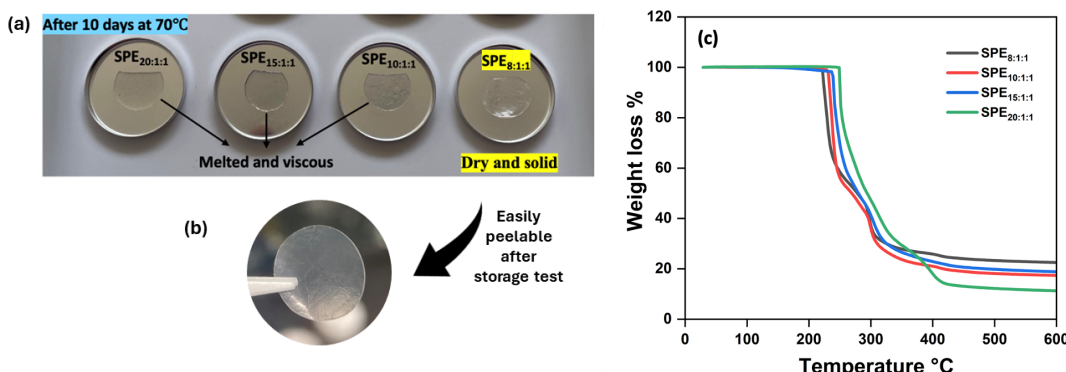
3.3 Dimensional and Thermal Stability

Figure 4. (a) and (b) Thermal storage experiment and (c) Thermal stability of the prepared PiHCIL-SPEs

As Li^+ conduction in SPEs mainly relies on chain segmental motion within the polymer's amorphous regions, high salt concentration that leads to increased amorphous domains therefore facilitates faster ion transport, owing to its plasticizing effect.[44] However, this increase in ion conductivity often comes at the expense of mechanical robustness due to reduced crystallinity and increased segmental motion. This dynamic shifts with our PiHCIL-SPEs, where membrane robustness is not solely reliant on the crystalline domains. Conducting a simple storage experiment at 70 °C provides valuable insights into mechanical stability, as depicted in Figure 4a. After 10 days storage at 70 °C, all SPEs above 8:1:1 ratio lost their dimensional integrity to some extent because of the existence of crystalline domains, as shown in the DSC results in **Figure 2c**, whereas $SPE_{8:1:1}$ remained in its original shape and integrity in **Figure 4b**. Hence, despite the absence of crystalline regions, $SPE_{8:1:1}$ shows high structural stability under elevated temperatures, pointing to sufficient mechanical robustness to prevent thermal deformation and potential Li dendrites penetration. Furthermore, thermal stability of SPEs is important for safe battery operation. **Figure 4c** presents the TGA results of the PiHCIL-SPEs. The negligible weight loss below 150 °C is ascribed to trapped moisture. The weight loss between 150 and 220 °C is because of the initial breakdown of LiFSI.[45] Extensive decomposition of the SPE started at above 220 °C. Adding LiFSI salt sped up the thermal breakdown of PiHCIL-SPEs.[46] Nevertheless, the PiHCIL-SPEs are still stable enough for safe use in solid-state LMBs
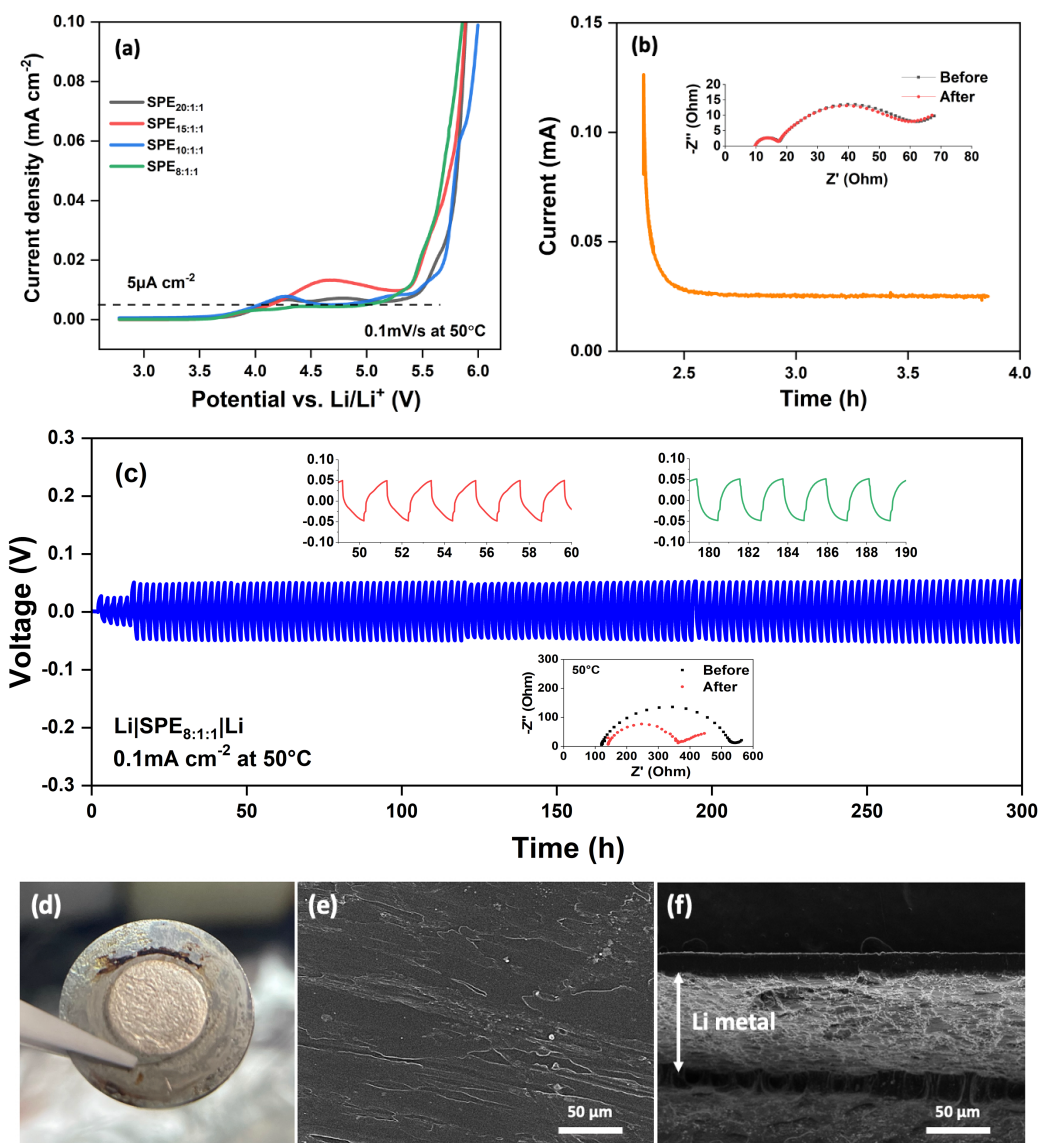
3.4 Electrochemical stability

Figure 5. (a) Electrochemical stability of the prepared PiHCIL-SPEs. (b) Change of current and impedance with time in symmetric Li|SPE8:1:1|Li cell under polarization at 10 mV and 70 °C. (c) Li||Li symmetric cell cycling of SPE8:1:1. (d-f) The surface image, surface morphology and cross-section SEM images of Li metal electrode (plated) after 150 cycles.

The electrochemical stability window (ESW) of the PiHCIL-SPEs was obtained by LSV measurement of a Li||SS cell, scanning from open-circuit voltage to 6 V against Li/Li$^+$ at a rate of 0.1 mV s^{-1} as shown in **Figure 5a**. Apart from SPE$_{8:1:1}$, all the other SPEs experienced oxidative degradation below 4 V which is commonly seen in PEO-based SPEs,[9] whereas SPE$_{8:1:1}$ showed high electrochemical stability of 5.1 V (5 μA cm^{-2} current density was used as the cut-off current [47]), indicating its excellent oxidation stability and potential to work with high-voltage materials. The excellent electrochemical stability of SPE$_{8:1:1}$ can be attributed to a high concentration of HCIL, promoting the polymer chains to strongly interact with Li$^+$ ions and FSI$^-$ anion clusters.[48] The coordinated ions and surrounded ion clusters act like a shield, protecting EO from oxidation and reducing the highest occupied molecular orbital level of the PiHCIL-SPE,[26,49] all of which contribute to

its improved oxidation stability. Thereby the $SPE_{8:1:1}$ has been chosen as the best candidate among others and will be investigated for the advanced electrochemical testing that will be discussed below.

Li transference number (t_{Li+}) of the $SPE_{8:1:1}$ was measured using a Li|Li symmetric cell at 70 °C. Figure 5b displays the current profile following a 10 mV polarization and the insert shows the impedances of the initial state and steady state. The t_{Li+} of $SPE_{8:1:1}$ was calculated to be 0.2 which is consistent with the typical PEO system and the HCIL electrolyte.[23] Ionic conduction in PEO-based SPEs is attributed to the chain segmental motion,[50,51] where Li^+ ions coordinates with the ether oxygen on PEO backbone, leading to Li dissociation.[52] However, Li^+ movements are restricted by the strong Li^+-EO coordination, which results in relatively low ionic conductivity and low t_{Li+} (around 0.2 - 0.3).[53,54] Thereby, the transference number achieved by the $SPE_{8:1:1}$ falls within the well-accepted region supporting the previous literature reports.

The interface compatibility between Li metal and the optimum $SPE_{8:1:1}$ was evaluated by Li plating-stripping cycling test. The symmetric Li|$SPE_{8:1:1}$|Li cell was cycled at constant current densities of 0.1 mA cm^{-2} for 1 hour polarisation at each step at 50 °C. As shown in **Figure 5c**, the long-term cycling of the Li|$SPE_{8:1:1}$|Li cell showed very stable performance with an overpotential of 50 mV over 150 cycles at 50 °C, and there was no sign of short circuit, indicating that $SPE_{8:1:1}$ has good compatibility with Li metal anode. The interfacial resistance decreased after 150 cycles (insert in **Figure 5c**), indicating that the $SPE_{8:1:1}$ continually adjusted to enhance its contact with the lithium surface. The surface image and morphology of Li metal after 150 cycles is shown in **Figure 5d-f**. A smooth and dense Li metal surface was observed with no signs of Li dendrites or dead Li, indicating a uniform Li deposition process and the formation of a stable SEI layer. The cross-section SEM of the platted side displayed a uniform and dense interface, which confirmed the excellent mechanical and electrochemical properties of $SPE_{8:1:1}$ that allows it to accommodate volume changes of the Li anode, thereby sustaining facile and reversible Li plating–stripping.

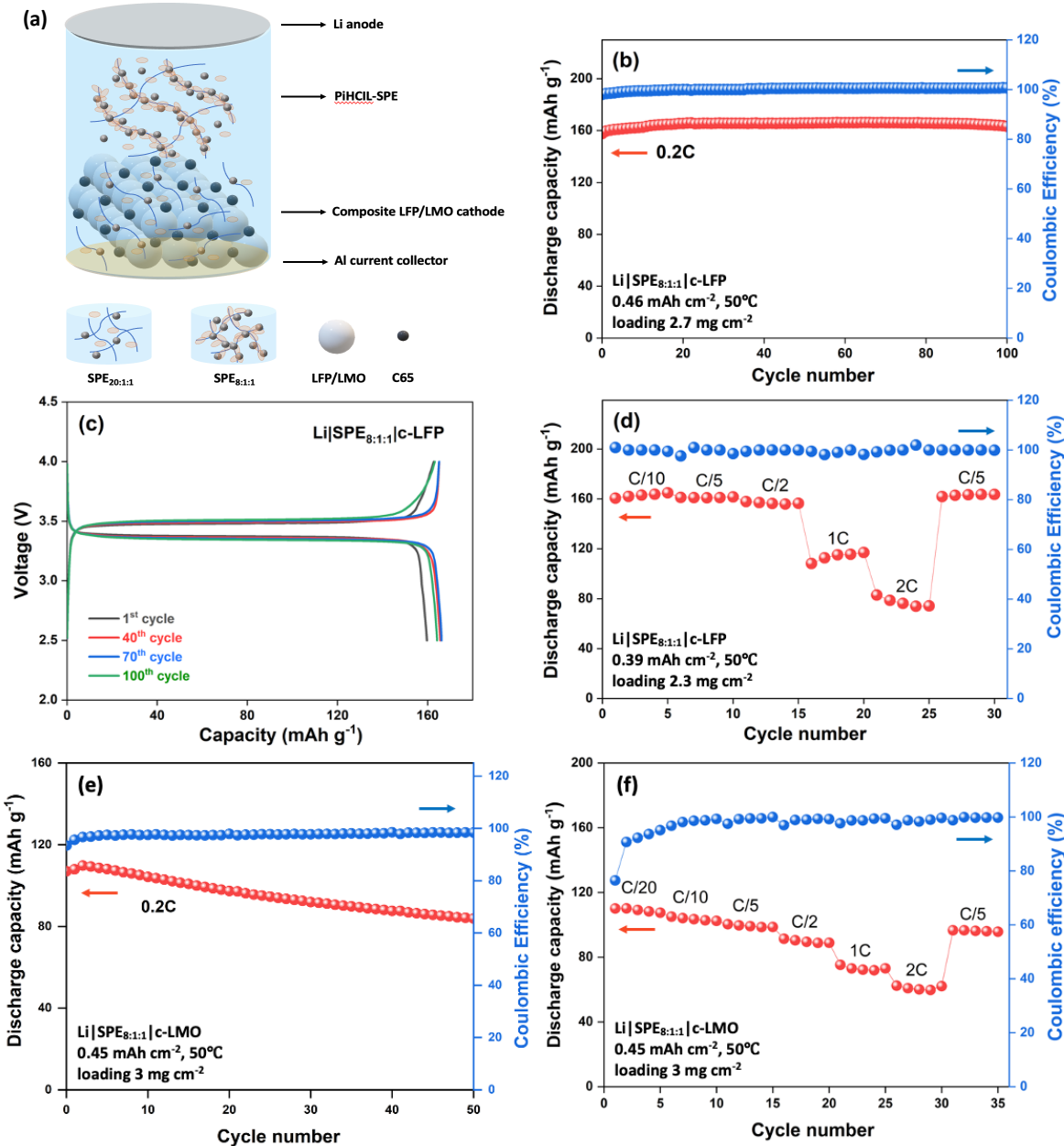## 3.5 All solid-state LMB full cell cycling

Figure 6. (a) Schematic illustration of the assembled all-solid-state Li|SPE$_{8:1:1}$|c-LFP/c-LMO cell. (b) Cycling performance of Li|SPE$_{8:1:1}$|c-LFP (2.7 mg cm^{-2}) cell cycled at C/5 rate (or 0.2 C) between 2.5–4.0 V for 100 cycles. (c) Charge-discharge profiles of different cycle numbers at C/5 rate. (d) Rate performances of Li|SPE$_{8:1:1}$|c-LFP cell (2.3 mg cm^{-2}) at different C rates. (e) Cycling performance of Li|SPE$_{8:1:1}$|c-LMO (3 mg cm^{-2}) cell cycled at C/5 rate between 3–4.3 V for 50 cycles. (f) Rate performances of Li|SPE$_{8:1:1}$|c-LMO cell (3 mg cm^{-2}) at different C rates.

The prepared all-solid-state Li|SPE$_{8:1:1}$|c-LFP/c-LMO cell is illustrated in **Figure 6a.** **Figure 6b** presents the cycling performance of the Li|SPE$_{8:1:1}$|c-LFP cell, which was cycled at C/5 rate at 50 °C between 2.5 and 4 V. The c-LFP cathode was prepared using the designed SPE as the binder to maintain the Li percolation within the cathode structure (more details are mentioned in the experimental section). Thereby the LMB constructed here is all-solid-state avoiding any trace of liquid wetting and the cell delivered 160 mAh g^{-1} initial discharge capacity. The performance then increased to 165 mAh g^{-1} after 20

cycles and stabilized, demonstrating the self-adaptability of $SPE_{8:1:1}$ membrane over cycling. After 100 cycles, the cell maintained an exceptional capacity retention of 99.2% and achieved nearly 100% coulombic efficiency (CE) throughout cycling. Other works are summarized in supplementary **Table S1** which clearly outlines the novelty of our PiHCIL-$SPE_{8:1:1}$ membrane and thereby suggests an impressive performance in comparison with the existing literature using similar cathode active loading and applied current density. Charge-discharge profiles at various cycle numbers are displayed in **Figure 6c**. The polarization remains low (180 mV) after 100 cycles, demonstrating the high stability of $SPE_{8:1:1}$. AC impedance profiles (**Fig. S5a**) showed an initial increase due to SEI formation, and after 40 cycles, the impedance slowly increases due to interface stability. A rate capability test was conducted at C/10, C/5, C/2,1C, 2C and C/5 current rates (1C is 0.4 mA cm^{-2}) as shown in **Figure 6d**. The Li|$SPE_{8:1:1}$|c-LFP cell showed 162, 159 and 155 mAh g^{-1} discharge capacities under C/10, C/5 and C/2 rate, respectively. It can maintain 47.3% discharge capacity when the current density is increased twentyfold from C/10 to 2C, indicating that the all-solid-state Li|$SPE_{8:1:1}$|c-LFP cell has an excellent tolerant to high current rate. The charge-discharge profiles at different C-rates are shown in **Fig. S6a**. The excellent rate performance indicated that $SPE_{8:1:1}$ have close contact with both Li and LFP electrodes to facilitate effective Li^+ transport and low interfacial resistance between the $SPE_{8:1:1}$ and cathode.[55]

To assess the potential for wider applications of the prepared PiHCIL-SPEs working with high voltage materials, we assembled Li||c-LMO cells with a cathode loading of 3 mg cm^{-2} with $SPE_{8:1:1}$. **Figure 6e** illustrates the cycling performance of the Li|$SPE_{8:1:1}$|c-LMO cell at 0.2C in the voltage range between 3 and 4.3 V. The Li|$SPE_{8:1:1}$|c-LMO cell maintain 80% discharge capacity after 50 cycles and interfacial resistance (**Fig. S5b**) slowly increases through cycling. **Fig. S6b** presents the charge–discharge profiles at different cycle numbers. The capacity decay maybe due to the dissolution of unstable manganese in LMO which is a common issue of high manganese active materials. The cell was further subjected to a rate capability test at various rates from C/20 to 2 C as show in **Figure 6f.** The SPE shows satisfactory discharge capacity retention of 55% from C/20 to 2C, demonstrating superior tolerance to high current rate. The exceptional rate performance and cycling stability of the Li|$SPE_{8:1:1}$|c-LMO cell confirms the potential of the designed SPE to work with high voltage cathodes and further applications to high energy storage systems.

4. Conclusion

In this study, we report the first use of a "high salt concentration ionic liquid" electrolyte with high molecular weight PEO to form high-performance solid polymer electrolytes, and their application in all-solid-state lithium metal batteries. These designed electrolytes are featured with unique interconnected and locally aligned ion clusters and pores that provide extra Li^+ ion transport pathways, leading to both high room temperature ionic conductivity and wide ESW. Benefiting from the organized structure change and increased ion dynamics by adding concentrated IL, ionic conductivity of 5.6 $x10^{-4}$ S cm^{-1} at 30°C is achieved with the optimal composition. Further FTIR and solid-state MAS NMR investigations confirm that these promising behaviors can be ascribed to a Li^+ environment change including increased Li^+-FSI^- interactions and weakened Li^+-EO interactions, leading to the formation of interconnected ion clusters as a distinct phase. The coordinated ions and surrounded ion clusters protect EO from oxidation, leading to improved oxidation stability (5.1 V). The novel PiHCIL-SPE provide stable Li symmetric cycling and promising electrochemical performance with a composite LFP cathode using the designed PiHCIL-SPE as the binder material, reflecting the superiority of the "PEO-in-HCIL" strategy. The implications of this

research bring a new understanding of PEO-based SPEs, promising not only to advance the field of all-solid-state LMBs but also to contribute to the broader pursuit of sustainable and high-performance energy storage solutions.

Credit authorship contribution statement

Mingjie Zhang carried out the experiments, analyzed the data and wrote the original manuscript. **Urbi Pal** conceived and mentored the research and revised the manuscript. **Faezeh Makhlooghiazad** mentored and revised the manuscript. **Shinji Kondou** helped in IR data analysis. **Luke A. O'Dell** helped to carry out the NMR measurements. **Claudio Gerbaldi** co-conceived the project and revised the manuscript. **Maria Forsyth** co-conceived and supervised the research and revised the manuscript. All the authors discussed the test results and put forward comments on the manuscript.

Acknowledgements

References

1. Janek, J. & Zeier, W. G. A solid future for battery development. *Nat. Energy* **1**, 16141 (2016).

2. Meyer, W. H. Polymer Electrolytes for Lithium-Ion Batteries. *Adv. Mater.* **10**, 439–448 (1998).

3. Song, Z. *et al.* A reflection on polymer electrolytes for solid-state lithium metal batteries. *Nat. Commun.* **14**, 4884 (2023).

4. Cheng, X., Pan, J., Zhao, Y., Liao, M. & Peng, H. Gel Polymer Electrolytes for Electrochemical Energy Storage. *Adv. Energy Mater.* **8**, 1702184 (2018).

5. Wang, X. *et al.* Gelled microporous polymer electrolyte with low liquid leakage for lithium-ion batteries. *J. Membr. Sci.* **454**, 298–304 (2014).

6. Qin, B. *et al.* Single-ion dominantly conducting polyborates towards high performance electrolytes in lithium batteries. *J. Mater. Chem. A* **3**, 7773–7779 (2015).

7. Fenton, D. E., Parker, J. M. & Wright, P. V. Complexes of alkali metal ions with poly(ethylene oxide). *Polymer* **14**, 589 (1973).

8. Armand, M. Polymer solid electrolytes - an overview. *Solid State Ion.* **9–10**, 745–754 (1983).

9. Xiao, S., Ren, L., Liu, W., Zhang, L. & Wang, Q. High-voltage polymer electrolytes: Challenges and progress. *Energy Storage Mater.* **63**, 102970 (2023).

10. Yusim, Y. *et al.* Evaluation and Improvement of the Stability of Poly(ethylene oxide)-based Solid-state Batteries with High-Voltage Cathodes. *Angew. Chem. Int. Ed.* **62**, e202218316 (2023).

11. Chen, L. *et al.* PEO/garnet composite electrolytes for solid-state lithium batteries: From "ceramic-in-polymer" to "polymer-in-ceramic". *Nano Energy* **46**, 176–184 (2018).

12. Song, X. *et al.* Unraveling the Synergistic Coupling Mechanism of Li $^+$ Transport in an "Ionogel-in-Ceramic" Hybrid Solid Electrolyte for Rechargeable Lithium Metal Battery. *Adv. Funct. Mater.* **32**, 2108706 (2022).

13. Zhang, X. *et al.* Vertically Aligned and Continuous Nanoscale Ceramic–Polymer Interfaces in Composite Solid Polymer Electrolytes for Enhanced Ionic Conductivity. *Nano Lett.* **18**, 3829–3838 (2018).

14. Shin, J.-H., Henderson, W. A., Scaccia, S., Prosini, P. P. & Passerini, S. Solid-state Li/LiFePO4 polymer electrolyte batteries incorporating an ionic liquid cycled at 40°C. *J. Power Sources* **156**, 560–566 (2006).

15.   Chen, Y. *et al.* Hyperbranched PEO-Based Hyperstar Solid Polymer Electrolytes with Simultaneous Improvement of Ion Transport and Mechanical Strength. *ACS Appl. Energy Mater.* **2**, 1608–1615 (2019).

16.   Gomez, E. D. *et al.* Effect of Ion Distribution on Conductivity of Block Copolymer Electrolytes. *Nano Lett.* **9**, 1212–1216 (2009).

17.   Zhang, H. *et al.* Single lithium-ion conducting solid polymer electrolytes: advances and perspectives. *Chem. Soc. Rev.* **46**, 797–815 (2017).

18.   Bouchet, R. *et al.* Single-ion BAB triblock copolymers as highly efficient electrolytes for lithium-metal batteries. *Nat. Mater.* **12**, 452–457 (2013).

19.   Porcarelli, L., Gerbaldi, C., Bella, F. & Nair, J. R. Super Soft All-Ethylene Oxide Polymer Electrolyte for Safe All-Solid Lithium Batteries. *Sci. Rep.* **6**, 19892 (2016).

20.   Kim, G. T. *et al.* UV cross-linked, lithium-conducting ternary polymer electrolytes containing ionic liquids. *J. Power Sources* **195**, 6130–6137 (2010).

21.   Armand, M., Endres, F., MacFarlane, D. R., Ohno, H. & Scrosati, B. Ionic-liquid materials for the electrochemical challenges of the future. *Nat. Mater.* **8**, 621–629 (2009).

22.   Howlett, P. C., MacFarlane, D. R. & Hollenkamp, A. F. High Lithium Metal Cycling Efficiency in a Room-Temperature Ionic Liquid. *Electrochem. Solid-State Lett.* **7**, A97 (2004).

23.   Yoon, H., Howlett, P. C., Best, A. S., Forsyth, M. & MacFarlane, D. R. Fast Charge/Discharge of Li Metal Batteries Using an Ionic Liquid Electrolyte. *J. Electrochem. Soc.* **160**, A1629–A1637 (2013).

24.   Matsumoto, H. *et al.* Fast cycling of Li/LiCoO2 cell with low-viscosity ionic liquids based on bis(fluorosulfonyl)imide [FSI]−. *J. Power Sources* **160**, 1308–1313 (2006).

25.   Susan, Md. A. B. H., Kaneko, T., Noda, A. & Watanabe, M. Ion Gels Prepared by in Situ Radical Polymerization of Vinyl Monomers in an Ionic Liquid and Their Characterization as Polymer Electrolytes. *J. Am. Chem. Soc.* **127**, 4976–4983 (2005).

26.   Suo, L. *et al.* "Water-in-salt" electrolyte enables high-voltage aqueous lithium-ion chemistries. *Science* **350**, 938–943 (2015).

27.   Wang, J. *et al.* Superconcentrated electrolytes for a high-voltage lithium-ion battery. *Nat. Commun.* **7**, 12032 (2016).

28.   Yoshida, K. *et al.* Oxidative-Stability Enhancement and Charge Transport Mechanism in Glyme–Lithium Salt Equimolar Complexes. *J. Am. Chem. Soc.* **133**, 13121–13129 (2011).

29.   Yamada, Y. & Yamada, A. Review—Superconcentrated Electrolytes for Lithium Batteries. *J. Electrochem. Soc.* **162**, A2406–A2423 (2015).

30.   Al-Masri, D., Yunis, R., Hollenkamp, A. F. & Pringle, J. M. Designing Solid-State Electrolytes through the Structural Modification of a High-Performing Ionic Liquid. *ChemElectroChem* **7**, 4118–4123 (2020).

31.   Pal, U. *et al.* Enhanced ion transport in an ether aided super concentrated ionic liquid electrolyte for long-life practical lithium metal battery applications. *J. Mater. Chem. A* **8**, 18826–18839 (2020).

32.   Pal, U. *et al.* Improved Li-Ion Transport by DME Chelation in a Novel Ionic Liquid-Based Hybrid Electrolyte for Li–S Battery Application. *J. Phys. Chem. C* **122**, 14373–14382 (2018).

33.   Pal, U. *et al.* Interphase control for high performance lithium metal batteries using ether aided ionic liquid electrolyte. *Energy Environ. Sci.* **15**, 1907–1919 (2022).

34.   Jin, L. *et al.* Structure and Transport Properties of a Plastic Crystal Ion Conductor: Diethyl(methyl)(isobutyl)phosphonium Hexafluorophosphate. *J. Am. Chem. Soc.* **134**, 9688–9697 (2012).

35.   Homann, G., Stolz, L., Neuhaus, K., Winter, M. & Kasnatscheew, J. Effective Optimization of High Voltage Solid-State Lithium Batteries by Using Poly(ethylene oxide)-Based Polymer Electrolyte with Semi-Interpenetrating Network. *Adv. Funct. Mater.* **30**, 2006289 (2020).

36.   Yang, J. *et al.* Crosslinked polymer-in-salt solid electrolyte with multiple ion transport paths for solid-state lithium metal batteries. *Energy Storage Mater.* **64**, 103088 (2024).

37.   Gao, H., Grundish, N. S., Zhao, Y., Zhou, A. & Goodenough, J. B. Formation of Stable Interphase of Polymer-in-Salt Electrolyte in All-Solid-State Lithium Batteries. *Energy Mater. Adv.* **2021**, 2021/1932952 (2021).

38.   Forsyth, M., Sun, J., Macfarlane, D. R. & Hill, A. J. Compositional dependence of free volume in PAN/LiCF3SO3 polymer-in-salt electrolytes and the effect on ionic conductivity. *J. Polym. Sci. Part B Polym. Phys.* **38**, 341–350 (2000).

39.   Yoon, H., Best, A. S., Forsyth, M., MacFarlane, D. R. & Howlett, P. C. Physical properties of high Li-ion content N-propyl-N-methylpyrrolidinium bis(fluorosulfonyl)imide based ionic liquid electrolytes. *Phys. Chem. Chem. Phys.* **17**, 4656–4663 (2015).

40.   Bar, N., Basak, P. & Tsur, Y. Vibrational and impedance spectroscopic analyses of semi-interpenetrating polymer networks as solid polymer electrolytes. *Phys. Chem. Chem. Phys.* **19**, 14615–14624 (2017).

41.   Dissanayake, M. A. K. L. & Frech, R. Infrared Spectroscopic Study of the Phases and Phase Transitions in Poly(ethylene oxide) and Poly(ethylene oxide)-Lithium Trifluoromethanesulfonate Complexes. *Macromolecules* **28**, 5312–5319 (1995).

42.   Dai, Y. *et al.* Lithium-7 NMR studies of concentrated LiI/PEO-based solid electrolytes. *Solid State Ion.* **106**, 25–32 (1998).

43.   Wu, N. *et al.* Fast Li [+] Conduction Mechanism and Interfacial Chemistry of a NASICON/Polymer Composite Electrolyte. *J. Am. Chem. Soc.* **142**, 2497–2505 (2020).

44.   Henderson, W. A. Crystallization Kinetics of Glyme−LiX and PEO−LiX Polymer Electrolytes. *Macromolecules* **40**, 4963–4971 (2007).

45.   Kerner, M., Plylahan, N., Scheers, J. & Johansson, P. Thermal stability and decomposition of lithium bis(fluorosulfonyl)imide (LiFSI) salts. *RSC Adv.* **6**, 23327–23334 (2016).

46.   Nguyen, H. T. T. *et al.* Facile Li [+] Transport in Interpenetrating O- and F-Containing Polymer Networks for Solid-State Lithium Batteries. *Adv. Funct. Mater.* **33**, 2213469 (2023).

47.   Herbers, L. *et al.* The Influence of Polyethylene Oxide Degradation in Polymer-Based Electrolytes for NMC and Lithium Metal Batteries. *Adv. Energy Sustain. Res.* **4**, 2300153 (2023).

48.   Xiong, Z. *et al.* 4.2V polymer all-solid-state lithium batteries enabled by high-concentration PEO solid electrolytes. *Energy Storage Mater.* **57**, 171–179 (2023).

49.   Wu, H. *et al.* A Polymer-in-Salt Electrolyte with Enhanced Oxidative Stability for Lithium Metal Polymer Batteries. *ACS Appl. Mater. Interfaces* **13**, 31583–31593 (2021).

50.   Johansson, P., Tegenfeldt, J. & Lindgren, J. Modelling amorphous lithium salt–PEO polymer electrolytes: ab initio calculations of lithium ion–tetra-, penta- and hexaglyme complexes. *Polymer* **40**, 4399–4406 (1999).

51. Molinari, N., Mailoa, J. P. & Kozinsky, B. Effect of Salt Concentration on Ion Clustering and Transport in Polymer Solid Electrolytes: A Molecular Dynamics Study of PEO–LiTFSI. *Chem. Mater.* **30**, 6298–6306 (2018).

52. Ratner, M. A. & Shriver, D. F. Ion transport in solvent-free polymers. *Chem. Rev.* **88**, 109–124 (1988).

53. Zhang, H. *et al.* Lithium bis(fluorosulfonyl)imide/poly(ethylene oxide) polymer electrolyte. *Electrochimica Acta* **133**, 529–538 (2014).

54. Itoh, T., Fujita, K., Uno, T. & Kubo, M. Polymer electrolytes based on vinyl ethers with various EO chain length and their polymer electrolytes cross-linked by electron beam irradiation. *Ionics* **23**, 257–264 (2017).

55. Tatara, R. *et al.* The Effect of Electrode-Electrolyte Interface on the Electrochemical Impedance Spectra for Positive Electrode in Li-Ion Battery. *J. Electrochem. Soc.* **166**, A5090–A5098 (2019).